Jahn-Teller distortion of C_{60}^- in $(Ph_4As)_2ClC_{60}$: C_{2h} versus C_i symmetry

V. C. Long* and E. C. Schundler
Department of Physics and Astronomy, Colby College, Waterville, Maine 04901, USA

G. B. Adams† and J. B. Page‡
Department of Physics and Astronomy, Arizona State University, Tempe, Arizona 85287, USA

W. Bietsch and I. Bauer
University of Bayreuth, Laboratory of Experimental Physics II and BIMF, D-95440 Bayreuth, Germany
(Received 13 September 2006; revised manuscript received 22 December 2006; published 1 March 2007)

We report a combined experimental and theoretical study of the on-ball vibrations of the singly charged C_{60} anion. The experimental material is $(Ph_4As)_2ClC_{60}$, a prototypical system for studying isolated C_{60}^-, which we have investigated by high-resolution infrared spectroscopy in the range 50–1500 cm^{-1} between 6 and 300 K. Our first-principles quantum molecular dynamics calculations provide complementary information on the vibrational spectra as well as simulated structural information about the reduced-symmetry cage. Our combined results indicate either C_{2h} or C_i symmetry for the Jahn-Teller distorted cage. In both cases, the cage is prolate and elongated along an axis that penetrates opposing five-membered rings. Bond-length changes are less than 0.013 Å. Observed temperature-dependent frequency shifts of the C_{60}^- vibrations are insufficient to identify any ordering transition, although low-temperature softening of a $T_{1u}(4)$-derived mode is substantial.

DOI: 10.1103/PhysRevB.75.125402 PACS number(s): 78.30.Na, 33.20.Ea, 33.20.Tp, 61.48.+c

I. INTRODUCTION

Charge transfer salts of C_{60}, in which the fullerene molecule gains one or more excess electrons, exhibit a variety of fascinating phenomena in which Jahn-Teller (JT) coupling[1,2] between electronic and vibrational energy levels plays a crucial role.[3,4] In the superconducting A_3C_{60} salts (A=alkali metal), the exact mechanism of superconductivity is still being clarified,[5,6] but the importance of the JT effect has long been acknowledged.[7,8] Although the A_4C_{60} compounds are insulating, their electronic properties are also attributed to aspects of JT electron-vibrational coupling.[3,9] In the organic ferromagnet tetrakis-dimethylaminoethylene (TDAE)-C_{60},[10] the orbital (orientational) ordering of closely spaced Jahn-Teller distorted cages, known as the cooperative JT effect, is believed to produce the ferromagnetic exchange.[11–17]

Although cooperative effects among JT-distorted C_{60} anions are assumed to play a crucial role in the properties of these materials, evidence of the actual distortion is usually indirect and often ambiguous.[18] Nuclear magnetic resonance (NMR) data of TDAE-C_{60} indicate a beltlike distribution of the electron density associated with a Jahn-Teller elongation of the cage,[19] and the contact configuration between neighboring cages appears to be crucial,[20] but the actual distortion symmetry of the cage has not been experimentally determined. Among the A_4C_{60} compounds, only in Cs_4C_{60}, which makes a transition to a cooperative JT state at low temperature, was structural evidence found for a distortion of the cage (D_{2h} in this case).[21] Structural investigations searched for a JT distortion of the C_{60}^{4-} cage in K_4C_{60} and Rb_4C_{60}, but succeeded only in excluding distortions greater than 0.04 Å.[22]

In the case of an intramolecular dynamic JT effect in charged C_{60},[2] structural investigations are not expected to observe the distortion, because the ball averages to high symmetry over very short time scales.[23] If the distortion is stabilized by crystal field interactions, however (a "static JT effect"),[2] the reduced cage symmetry can sometimes be determined by x-ray diffraction. Two materials were found to exhibit discernible structural distortions due to a suppression of orientational disorder and a static JT effect: $[PPN^+]_2C_{60}^{2-}$ with a C_i-distorted prolate cage,[24] $[Ni(C_5Me_5)_2^+][C_{60}^-]CS_2$ with a C_{2h} oblate cage.[25] On the theoretical side, some investigations of the molecular JT effect in C_{60}^{n-} have been limited to linear JT coupling;[26,27] while others[23,28–30] incorporated higher-order terms, producing a likely D_{5d} or D_{3d} cage distortion. C_{60}^- has also been investigated by *ab initio* electronic-structure-based numerical simulations. The earliest of these simulations were either constrained[31] to three subgroups of the icosahedral group, namely D_{5d}, D_{3d}, and D_{2h}, or else found the lowest-energy distortion without any consideration of symmetry.[32] A more recent simulation[33] finds a C_i distortion to be the likeliest symmetry of the singly charged cage.

As a complement to work on materials with strongly interacting C_{60} anions, salts of C_{60} with well-separated monoanions have been investigated in order to understand the JT effect in nearly isolated C_{60}^-. The isostructural set $(Ph_4X)_2YC_{60}$ (Ph=phenyl=C_6H_5; X=P and Y=I, Cl, or Br; or X=As and Y=Cl) has well-isolated C_{60}^- cages and the experimental advantage of being stable in air.[34,35] The crystal lattice of these materials is $I4/m$, with C_{60}^- and halide anions each at the center of a tetragonally distorted cube of Ph_4X cations.[33,34,36,37] A nearly cubic symmetry embrace of phenyl rings encapsulates each C_{60}^-,[35] with offset face-to-face or edge-to-face attractive interactions between Ph rings and C_{60} hexagons.[38] Since the fourfold crystallographic symmetry is not replicated in the I_h point group,[39] there are two equivalent perpendicular orientations of the C_{60}^- cage that are randomly occupied.[34,36,37] Although both the disorder and the JT

effect are reported to be static at low temperature,[36,40,41] no distortion of C_{60}^- in $(Ph_4X)_2YC_{60}$ has been detected by x-ray diffraction[34–37] or diffuse x-ray scattering,[42] and an upper bound of 0.01 Å has been set on deviations from an I_h symmetry cage.[36]

In addition to the structural studies, other experimental methods have been employed to clarify the properties of the C_{60} monoanion in the $(Ph_4X)_2YC_{60}$ set of materials.[33,40–58] Of particular relevance for this paper is a previous vibrational study of $(Ph_4P)_2IC_{60}$ which found splitting of the T_{1u} C_{60} modes and activation of silent vibrations, consistent with a D_{5d} or D_{3d} JT distortion of the cage.[55] Although a JT distortion of C_{60}^- was successfully confirmed, the accuracy of the symmetry identification was limited because a strong counterion vibration obscures the region of the fundamental $T_{1u}(1)$ vibration and because no comparison was made to a calculated spectrum. A JT distortion of the C_{60}^- cage in $(Ph_4X)_2C_{60}Y$ materials also was revealed by angular-dependent electron spin resonance (ESR) studies, which found an anisotropic g factor at low T.[33,40,41,43] Among these studies, however, there was no consensus as to whether the specific distortion type was D_{2h}[40] or a lower symmetry such as C_{2h} or C_i[33] (note that neither choice is consistent with the conclusion of the vibrational study[55]). The description of the low-temperature state, the nature of a transition to that state, and the transition temperature have also been the subject of disagreement.[33,36,40,42,55]

Vibrational properties are highly sensitive to molecular symmetry. Recent combined experimental-theoretical vibrational studies of C_{60} polymers found considerable mixing of the isolated neutral I_hC_{60} modes (mode mixing) and surprisingly large mode splittings in spectra of the bonded distorted cages.[59–61] In light of those unexpected results, and to address the specific limitations of the earlier vibrational work on the isostructural fulleride salt,[55] we have undertaken a combined experimental-theoretical examination of the vibrational properties of $(Ph_4As)_2ClC_{60}$. Experimentally, $(Ph_4As)_2ClC_{60}$ has the advantage over $(Ph_4P)_2IC_{60}$ in that both $T_{1u}(1)$- and $T_{1u}(2)$-derived modes appear unobscured in the spectrum. We also wanted to address the inconsistencies of previous $(Ph_4X)_2C_{60}Y$ studies and the ongoing need for more information about JT distortions in charged C_{60}.[18]

After reviewing our experimental and calculational methods, we begin by identifying C_{60}^- modes in the experimental spectrum, then discuss the temperature (T) dependence of those modes. Next we focus on a comparison of the experimental spectrum with calculated spectra for differently distorted cages. Finally, we compare the geometry of the simulated structures with previous experimental results for both the lattice and the enclosed cage, and summarize our results.

II. MATERIALS AND METHODS

A. Experiments

Several batches of small single crystals of $(Ph_4As)_2ClC_{60}$ were prepared by electrocrystallization;[41] the quality of sample batches was confirmed at room temperature by ESR. The crystals were ground up with paraffin at 77 K or mixed with KBr at room temperature and pressed at 2000 or 20 000 psi under vacuum into homogeneous pellets for far infrared (FIR) or middle infrared (MIR) measurements. Concentrations were optimized between 0.6 and 2.5 % for various transmittance regions. Pellet samples were stored in evacuated desiccators.

High resolution (0.25 cm^{-1} for FIR, 0.5 cm^{-1} for MIR) transmittance spectra were taken with a Bruker IFS 66 V Fourier transform spectrometer. We found good reproducibility among varying sample concentrations and batches, although minor intensity changes occurred in some features after repeated temperature cycling or extended storage times. An Infrared Labs helium-cooled Si bolometer was used for far infrared data collection and a custom Janis cold gas cryostat provided stable temperature control between 6 K and 300 K. Reference scans through an identical sample mount hole were taken at each temperature. Discrepancies between thermometers mounted on the heater vaporizer and sample holder were generally much less than 10%; reported temperatures are from the sample holder thermometer with a small correction for the discrepancy. For this type of cold gas immersion cryostat with data taken as the temperature is stepwise increased, any error would likely make the actual sample temperature colder than the recorded temperature value.

We measured the low temperature spectra of $AsPh_4Cl$-H_2O and $AsPh_4Cl$-HCl to approximate the counterion of the fulleride salt. Sample pellets were prepared as described above. Intense broad H_2O peaks[62,63] between 500 and 600 cm^{-1} make the hydrate compound ill suited for comparison to the fulleride salt spectrum in the FIR, and our attempts to eliminate the water by vacuum drying failed. On the other hand, spectra of $AsPh_4Cl$-HCl provide a reasonable comparison for the purpose of identifying C_{60}^- modes below $\approx$700 cm^{-1}. Since the hydrate compound has fewer extra modes in the MIR than the HCl compound, the former was chosen for comparison to the fulleride salt in that region.

B. Calculations

Our method for these simulations of isolated C_{60}^- is the first-principles quantum molecular dynamics (QMD) of Sankey and Niklewski.[64] The method is characterized by three main approximations: the local density approximation (LDA), use of the non-self-consistent Harris energy functional, and expansion of the wave function in a minimal basis set of four pseudoatomic local orbitals (one s and three p). An important additional approximation is that the free-atom local orbitals are created with the boundary condition that their wave functions vanish at a "confinement radius" r_c of 4.1 Bohr radii; this approximation restricts the number of interacting neighbors of each atom in the molecule to the number within a radius of $2r_c$ (for example, each atom in I_h C_{60} has 21 interacting neighbors). The method has been well tested for carbon, for both neutral and charged fullerenes,[32,65,66] and for fullerene polymers,[59–61,67–70] as well as for nanotubes[71] and carbon solids.[32,72–74]

In our QMD method, equilibrium geometries are obtained by relaxing an approximate initial structure; the relaxation is

accomplished by imposing an artificial damping algorithm which removes excess kinetic energy as the atoms move towards the configuration having minimum potential energy. At each step in the relaxation, we obtain the charge density of the structure, as well as all atomic forces and the total energy. Our simulation of C_{60}^- begins by adding a single electron to a relaxed neutral I_h C_{60}. The initial relaxation of the resulting charged molecule lowers its energy by 0.013 eV without disturbing the I_h symmetry. We are then able to produce a C_{60}^- having any desired subgroup symmetry by providing a small random distortion (but having the desired symmetry) and again allowing the molecule to relax; during this relaxation the symmetry may increase, but cannot decrease (for example, the molecule might return to I_h symmetry), because the nonsymmetric force components sum to zero. Although the distorted C_{60}^- found by such a relaxation is guaranteed to have not less than the desired symmetry, we cannot insure that there are not other distorted C_{60}^- structures having the same symmetry and perhaps lower energy. In an effort to find an alternate distorted C_{60}^- having the same symmetry, at the end of each relaxation we multiply the final distortion by −1, apply this "inverted" distortion to I_h C_{60}^-, and rerelax. For example, the inversion of a prolate distortion will be oblate, and vice versa; however, the subsequent relaxation may then restore the original character of the distortion.

We have used this strategy to produce distorted C_{60}^- molecules having the subgroup symmetries D_{5d}, D_{3d}, D_{2h}, and C_{2h}. For each of the D_{2h}, D_{3d}, and D_{5d} symmetries, the strategy yields a low-energy distortion which is prolate and elongated along the major symmetry axis (either of the three C_2 axes in the D_{2h} case). For C_{2h} we find two energetically competitive distortions, $C_{2h,5}$ and $C_{2h,6}$, both of which are prolate, but neither of which is elongated along the C_2 axis; we describe these two distortions in detail in Sec. III D. In addition, we have produced another distortion by allowing a period of random room-temperature thermal vibrations followed by a relaxation; this results in a distorted C_{60}^- having C_i symmetry and an energy close to those for our other configurations. Although standard JT theory for a $T \otimes h$ Jahn-Teller system such as C_{60}^- does not lead to C_i (Ref. 2, Chap. 2), our simulations do not have these restrictions. Indeed, the experimentally relevant factors which determine the realizable molecular configurations are the kinetics during the sample growth. Hence the C_i distortion must be considered. The energies of all our distorted C_{60}^- molecules are essentially equal, approximately 0.046 eV (±0.003 eV) less than the energy of relaxed I_h C_{60}^-.

For the distorted molecules described above, the equilibrium atomic positions determined by our program cannot be regarded as unique. There are likely to be other sets of atomic positions having the same distortions (i.e., also prolate and with the same axes of elongation) and for which the net force on every atom is also zero. For the D_{2h}, $C_{2h,5}$, and C_i symmetries, by applying alternate initial distortions, we have produced multiple sets of equilibrium atomic positions for the purpose of estimating the uncertainty inherent in our comparison of vibrational experiment and theory (as discussed in greater detail in Sec. III C).

Once an equilibrium geometry of a desired symmetry is obtained, the normal modes are calculated in the harmonic approximation: one at a time, the atoms are given small displacements and the resulting QMD atomic forces per unit displacement yield the harmonic force constants. In the region 300–700 cm^{-1}, there are two IR-active modes and eleven non-IR-active I_h C_{60} modes; the frequencies we calculate for these modes are in excellent agreement with the corresponding experimental values,[75] giving us confidence in using our calculated C_{60}^- frequencies for comparison with experiment in this range. IR strengths are calculated within the linear electric-dipole-moment approximation: in this case, individual atoms are again given small displacements and the resulting QMD dipole moments per unit displacement yield the effective charges. The effective charges are multiplied by the normal mode displacements to produce the mode dipole moments, the squares of which give the relative areas of the modes' IR lines. These temperature-independent δ-function strengths are given Lorentzian broadening to produce a theoretical IR spectrum for each equilibrium geometry. As detailed in Sec. 2.3 of Ref. 75, our calculated IR intensities are much more uncertain than our calculated frequencies; hence, in our assignments we make only limited use of the intensity information, as described in Sec. III C.

III. RESULTS AND DISCUSSION

A. Identification of C_{60}^- features

The first task in understanding the vibrational data is to identify features attributable to the C_{60}^- anion, which we accomplish by comparing spectra of the fulleride salt $(Ph_4As)_2ClC_{60}$ and the appropriate counterion $AsPh_4Cl$-HCl or $AsPh_4Cl$-H_2O, as shown in Figs. 1(a) and 2(a). We assign C_{60}^- modes as those features present in the fulleride salt spectrum but missing in the counterion spectrum; they are marked by square dots in the figures. The identification of some features is ambiguous because of small frequency shifts or intensity differences between the two spectra. To aid in the assignment process, it is instructional to review known vibrations of molecular groups contained in the counterion and to compare our $(Ph_4As)_2ClC_{60}$ spectra with published data of the isostructural fulleride salt, $(Ph_4P)_2IC_{60}$, and its counterion, Ph_4PI.[55,58]

The large number of counterion features throughout the FIR and MIR are vibrational modes of the substituted phenyl rings (C_6H_5-X).[76–78] These vibrations consist of in- and out-of-plane deformations of the six-membered carbon rings and associated H atoms, as well as modes that involve significant movement of the substituted atom X (X=As or P in the two different versions of the fulleride salt), making those mode frequencies sensitive to the mass of X.[76] The X sensitivity accounts for significant differences between some phenyl ring modes in Ph_4PI and $AsPh_4Cl$-HCl, especially in the FIR region. Most notably, the strong phenyl ring vibration at 526 cm^{-1} that obscures the $T_{1u}(1)$-derived modes in $(Ph_4P)_2IC_{60}$ shifts away from that frequency in $(Ph_4As)_2ClC_{60}$, making the latter material a better choice for study of the fulleride anion vibrations. Because intramolecular modes of C_{60}^- should be relatively insensitive to the counterion environment, only when features not in the counterion

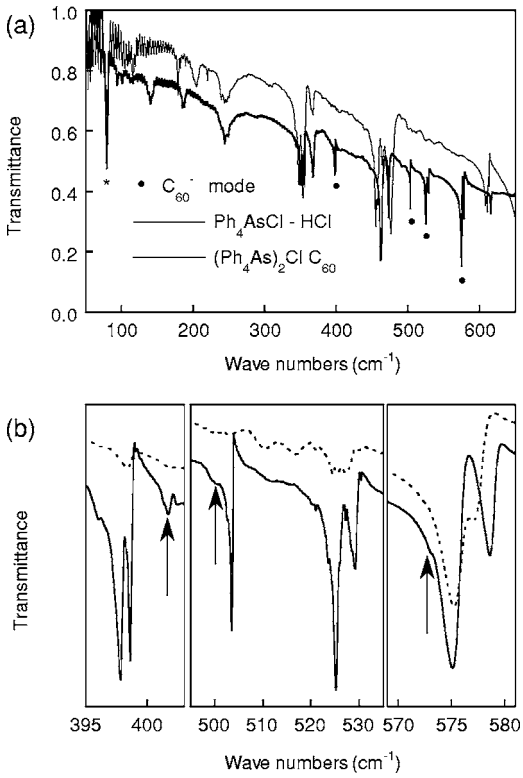

FIG. 1. (a) Far infrared low-temperature transmittance spectra of $(Ph_4As)_2ClC_{60}$ (T=6 K) and of the counterion $AsPh_4Cl$-HCl ($T \approx 40$ K), in pressed paraffin pellets. Both spectra exhibit interference fringes in the low wave number (frequency) region. C_{60}^- modes are marked with solid square dots. The asterisk indicates a paraffin mode. (b) Magnified views of C_{60}^- vibrational features in $(Ph_4As)_2ClC_{60}$ at room temperature (dashed) and T=6 K (solid). Arrows points to weak features whose identification is ambiguous.

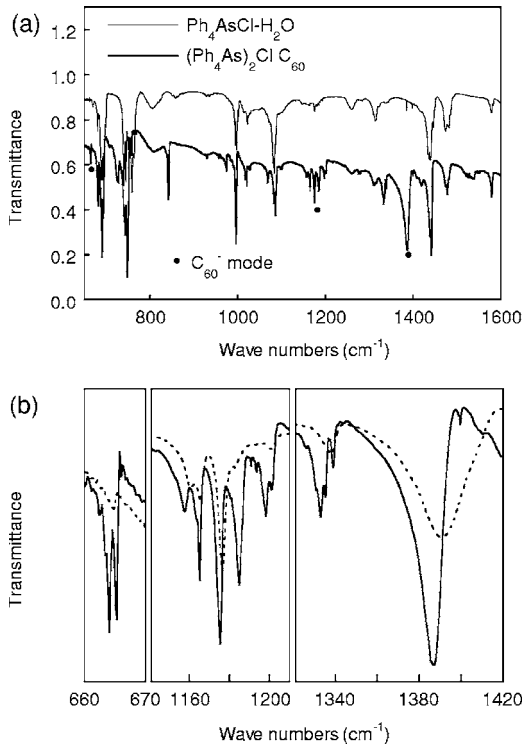

FIG. 2. (a) Middle infrared transmittance spectra at T=6 K of $(Ph_4As)_2ClC_{60}$ and of the counterion $AsPh_4Cl$-H_2O, in pressed paraffin pellets. C_{60}^- modes are marked with solid square dots. (b) Magnified views of C_{60}^- vibrational features in $(Ph_4As)_2ClC_{60}$ at room temperature (dashed) and T=6 K (solid).

spectrum are found at the same frequency in the two versions of the fulleride salt are they candidates for C_{60}^- vibrations. Since we are concerned with intramolecular C_{60}^- modes sensitive to the on-ball symmetry distortion, we do not attempt to assign features below 200 cm^{-1}.

Based on these considerations, we identify three sets of features positively attributable to C_{60}^- in the FIR spectrum (50–650 cm^{-1}) of $(Ph_4As)_2ClC_{60}$: a narrow doublet at 397.9 and 398.6 cm^{-1}, a widely split multiplet at 504, 525, and 529 cm^{-1}, and a strong doublet centered at 575.1 and 578.6 cm^{-1}. These features are shown magnified in Fig. 1(b). Each of these meets the above criterion for identifying C_{60}^- modes in $(Ph_4As)_2ClC_{60}$ and all are within 1 cm^{-1} of the corresponding observable C_{60}^- frequencies in $(Ph_4P)_2IC_{60}$,[55] except for the 529 cm^{-1} mode, which shifts by 3 cm^{-1}. These seven positively identified FIR C_{60}^- features are listed in column one of Table I.

Identification of C_{60}^- modes is more difficult in the MIR region (650–1500 cm^{-1}) due to the abundance of counterion phenyl ring modes throughout (Fig. 2). We are able to use the criterion for identifying C_{60}^- modes for a narrow doublet at 665 cm^{-1} (also listed in column one of Table I), a multiplet grouped near 1175 cm^{-1}, and a strong feature at 1387 cm^{-1}, all shown magnified in Fig. 2(b). Wide splitting of the 1387 cm^{-1} C_{60}^- mode probably accounts for some nearby features but remains unconfirmed because there are counterion modes in the same region. Although the 1175 cm^{-1} feature also overlaps with some weak counterion modes, its fivefold splitting [Fig. 2(b)] may be due solely to C_{60}^-, since it appears identically in $(Ph_4P)_2IC_{60}$.[58] Other potential C_{60}^- modes in this region appear at 727 and 974 cm^{-1} but are too close in frequency to counterion modes to assign with confidence. One puzzling feature is a sharp and moderately strong peak at 842 cm^{-1} that meets our criterion for C_{60}^- modes but has no recognizable counterpart in the calculated vibrations of C_{60}^-. This feature does occur, albeit somewhat more weakly, in the Ph_4PI counterion spectrum[58] and also as a weak multiplet in the MIR hydrochloride counterion spectrum (not shown), although not the hydrate counterion spectrum. It may be an activated phenyl ring mode, since it coincides with a known Raman-active Ph frequency (non-X-sensitive).[76]

As is evident by close inspection of the data in Figs. 1–3, the primary features of $(Ph_4As)_2ClC_{60}$ spectrum are overlaid by a large number of reproducible small sharp peaks (seen most clearly in Fig. 3), which we call the "fine structure." These small well-defined features appear throughout the FIR region in proximity to both C_{60}^- and counterion modes, and to a lesser extent in the MIR. Such fine structure appears to a much lesser degree in the pure counterion spectra. Because of the ubiquity of the fine structure and its presence in regions where no C_{60}^- modes are IR-active (such as between 400–500 cm^{-1}, see Table I), we conclude that such structure

TABLE I. Vibrational mode assignments for C_i- and $C_{2h,5}$-distorted C_{60}^-. Experimental frequencies (ν) (ambiguous C_{60}^- modes are in parentheses), calculated frequencies (an asterisk indicates the intensity is an order of magnitude less than that of other modes in the same symmetry group), errors, mode symmetries, and parent symmetries for each simulated distortion. The mode error=(calculated ν −experimental ν)/experimental ν; the average error is found from the magnitudes of the mode errors. Some of the $C_{2h,5}$ calculated frequencies are shown out of order so that assigned modes are in the same row for both symmetry cages.

	Simulated C_i					Simulated $C_{2h,5}$				
Experimental ν (cm^{-1})	ν (cm^{-1})	Error %	Mode symmetry	I_h parent symmetry	%	ν (cm^{-1})	Error %	Mode symmetry	I_h Parent symmetry	%
	329.0		A_u	$T_{3u}(1)$	96.8	328.6		B_u	$T_{3u}(1)$	98.1
	331.3		A_u	$T_{3u}(1)$	97.7	330.5		A_u	$T_{3u}(1)$	96.1
	331.8		A_u	$T_{3u}(1)$	97.4	332.6		B_u	$T_{3u}(1)$	96.4
	342.5		A_u	$G_u(1)$	96.8	342.5		A_u	$G_u(1)$	99.4
	343.7		A_u	$G_u(1)$	96.9	342.6		A_u	$G_u(1)$	96.4
	344.2		A_u	$G_u(1)$	98.4	343.1		B_u	$G_u(1)$	97.0
	345.2		A_u	$G_u(1)$	98.9	343.3		B_u	$G_u(1)$	97.6
397.8	390.7	−1.79	A_u	$H_u(1)$	99.6	391.7	−1.53	A_u	$H_u(1)$	99.8
398.6	392.7	−1.47	A_u	$H_u(1)$	99.7	392.2	−1.61	B_u	$H_u(1)$	99.3
(401.7)	395.9	−1.44	A_u	$H_u(1)$	99.7	395.4	−1.56	A_u	$H_u(1)$	99.7
	398.2*		A_u	$H_u(1)$	99.7	396.4*		B_u	$H_u(1)$	99.7
	401.2*		A_u	$H_u(1)$	99.9	400.0*		A_u	$H_u(1)$	99.7
(502.7)										
503.5	505.5	+0.39	A_u	$T_{1u}(1)$	99.2	505.8	+0.46	B_u	$T_{1u}(1)$	99.2
	515.7		A_u	$H_u(2)$	87.8	515.7*		A_u	$H_u(2)$	84.1
				$T_{1u}(1)$	8.8				$T_{1u}(1)$	13.9
	518.6*		A_u	$T_{1u}(1)$	50.0	519.4		A_u	$T_{1u}(1)$	67.5
				$H_u(2)$	48.0				$H_u(2)$	31.6
	519.9		A_u	$T_{1u}(1)$	58.5	520.8*		B_u	$T_{1u}(1)$	71.3
				$H_u(2)$	40.9				$H_u(2)$	27.0
	523.2		A_u	$H_u(2)$	62.8	525.5*		A_u	$H_u(2)$	96.5
				$T_{1u}(1)$	35.5					
525.2	524.2	−0.19	A_u	$H_u(2)$	60.9	522.6	−0.48	B_u	$H_u(2)$	72.0
				$T_{1u}(1)$	36.4				$T_{1u}(1)$	26.8
	526.8*		A_u	$H_u(2)$	97.8	525.9*		A_u	$H_u(2)$	97.9
529.2	527.0	−0.41	A_u	$H_u(2)$	90.5	523.7	−1.03	A_u	$H_u(2)$	82.3
				$T_{1u}(1)$	8.5				$T_{1u}(1)$	14.7
(573.0)	555.2	−3.11	A_u	$T_{1u}(2)$	96.0	555.5	−3.04	B_u	$T_{1u}(2)$	98.2
575.1	557.1	−3.13	A_u	$T_{1u}(2)$	94.6	556.5	−3.23	A_u	$T_{1u}(2)$	95.3
578.6	562.9	−2.71	A_u	$T_{1u}(2)$	99.4	559.3	−3.33	B_u	$T_{1u}(2)$	99.8
	644.3*		A_u	$H_u(3)$	99.4	643.6		B_u	$H_u(3)$	99.6
	644.9		A_u	$H_u(3)$	99.6	645.0		A_u	$H_u(3)$	99.7
	646.2		A_u	$H_u(3)$	99.7	645.3*		B_u	$H_u(3)$	99.1
664.1	652.0	−1.83	A_u	$H_u(3)$	99.3	647.5	−2.50	A_u	$H_u(3)$	99.6
665.2	654.2	−1.66	A_u	$H_u(3)$	99.5	651.1	−2.11	A_u	$H_u(3)$	99.3
	688.3*		A_u	$T_{3u}(2)$	97.2	687.3		B_u	$T_{3u}(2)$	92.4
	689.4*		A_u	$T_{3u}(2)$	93.0	687.6		A_u	$T_{3u}(2)$	95.2
	692.4		A_u	$T_{3u}(2)$	96.7	693.8		B_u	$T_{3u}(2)$	98.1
Average error		1.65					1.90			

is not due to the fulleride anion; perhaps it is due to some interaction that weakly activates counterion modes. We dismiss contamination as a source because the same fine structure appears in spectra of multiple sample pellets from $(Ph_4As)_2ClC_{60}$ samples grown in different years. Although published spectra[55] of the isostructural salt $(Ph_4P)_2IC_{60}$ show

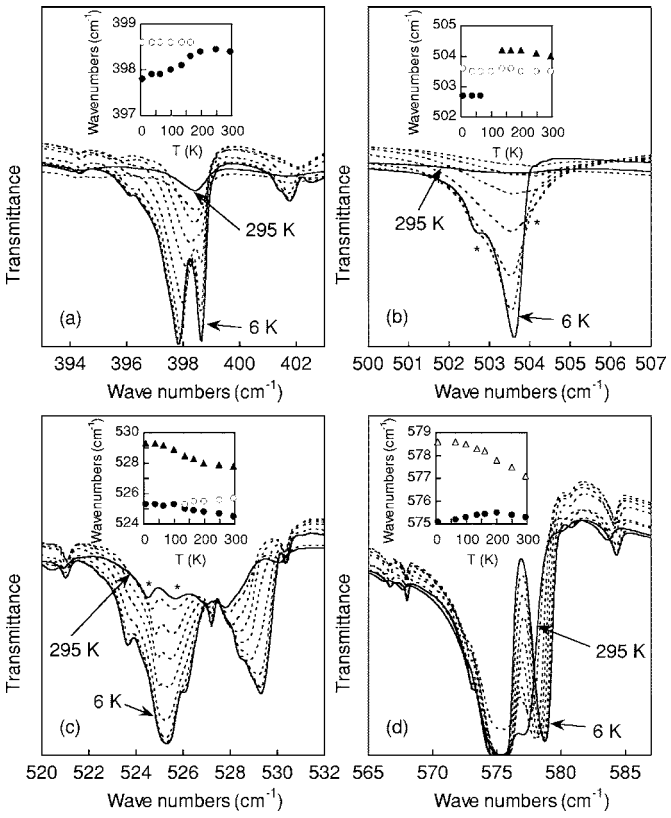

FIG. 3. (a)–(d) Temperature dependence of the C_{60}^- modes in $(Ph_4As)_2ClC_{60}$. Insets show the temperature-dependent shifts of the major inverted peak wave numbers (frequencies). Asterisks indicate weaker features also followed in the insets. The $T=248$ K spectrum has been shifted vertically to account for an offset artifact due to experimental conditions. (d) Since the peak is saturated due to the sample concentration, the wave numbers (frequencies) in the inset are taken from data on a lower concentration sample that allowed better determination of the peak minima.

almost no fine structure, it could be easily obscured by the large interference fringing and greater noise of that data. Since we cannot confidently discriminate between unidentified fine structure and weak features of C_{60}^-, we neglect the abundant fine structure and limit our discussion to the most intense vibrations. The few exceptions are indicated by arrows in Fig. 1(b): two small peaks, at 401.7 and 502.7 cm^{-1}, that occur in both fulleride salt spectra[79] adjacent to identified C_{60}^- features, and a rather rounded shoulder at 573 cm^{-1} (unlike the narrow fine-structure peaks). Since these three peaks are potential C_{60}^- features, they are listed in parentheses in column 1 of Table I.

B. Temperature dependence of C_{60}^- vibrations

We studied the detailed temperature dependence of the FIR C_{60}^- modes in $(Ph_4As)_2ClC_{60}$ in order to look for an ordering transition reported in previous vibrational,[55] structural,[36,42] and ESR studies[33,40,41,43,47] of the $(Ph_4X)_2YC_{60}$ materials. Figures 3(a)–3(d) show how the intensity and splitting of C_{60}^- modes develop with decreasing T. The insets trace the frequency changes with temperature of the inverted peak minima.

Figures 3(a)–3(c) show substantial increases in intensity and sharpness of the C_{60}^- peaks with decreasing T, as was observed previously in $(Ph_4P)_2IC_{60}$.[55] The narrow doublet splitting of the 398 cm^{-1} vibration below 200 K [Fig. 3(a)] strongly resembles the behavior of the same feature in $(Ph_4P)_2IC_{60}$, in which it splits below about 125 K.[55] In both materials, the lower frequency component softens (decreases in frequency) with decreasing T. The different splitting temperatures may be due to a combination of several factors: different ultimate splitting separation, slightly different measurement resolutions, and the thermometry of different cooling systems. Since both data sets appear to be resolution limited, an undetected doublet nature of this mode may persist to even higher temperatures, adding uncertainty to the assigned splitting temperatures.

The 504 cm^{-1} C_{60}^- mode [Fig. 3(b)] shows no frequency shift with T, although it sharpens and intensifies with decreasing T and has a T-dependent shoulder on each side. The C_{60}^- multiplet at 527 cm^{-1}, obscured in $(Ph_4P)_2IC_{60}$ data by a strong counterion mode,[55] shows complex behavior with decreasing T in $(Ph_4As)_2ClC_{60}$ [Fig. 3(c)]. At room temperature, this feature includes additional structures at 511 and 517 cm^{-1} [Fig. 1(b)] that disappear as T decreases and are replaced at low temperature by two major inverted peaks at 525 and 529 cm^{-1}, overlaid by multiple fine-structure features. The 525 cm^{-1} branch, formed by two merging modes, has little T-induced frequency shift, whereas the 529 cm^{-1} branch hardens (increases in frequency) with decreasing T below 200 K.

Figure 3(d) shows the strongest FIR C_{60}^- vibration in $(Ph_4As)_2ClC_{60}$, which consists of a doublet at 575.1 and 578.6 cm^{-1} plus a low-energy shoulder and other nearby fine structure. If the ambiguous shoulder at 573 cm^{-1} is taken to be an intrinsic part of the multiplet, it would make this C_{60}^- feature a triplet. The pronounced doublet splitting increases with decreasing T due to softening of the lower-energy branch and hardening of the higher branch. The softening of the lower-energy branch is not monotonic, however, but reverses an initial hardening trend below 200 K. The same type of reversal is exhibited by this mode in $(Ph_4P)_2IC_{60}$ around 150 K.[55]

We did not follow the temperature dependence of the MIR modes in detail because of the difficulty in positively identifying all the C_{60}^- modes. However, a comparison of the room-temperature and low-temperature data [Fig. 2(b)] reveals that both the 665 cm^{-1} narrow doublet and the 1175 cm^{-1} multiplet intensify and split increasingly with decreasing T, due to softening of several branches while others harden or remain at constant frequency. In contrast, the very strong 1387 cm^{-1} fullerene anion mode does not split, but downshifts more than any of the other modes, by 4 cm^{-1} from room temperature to 6 K.

Since the temperature-induced transition was suggested to be a bulk phenomenon,[55] we reviewed as well the temperature-dependent behavior of the counterion modes. In general, the low-T behavior of counterion modes in the fulleride salt is comparable to their behavior in the isolated counterion materials (not shown). Of the numerous counterion modes throughout the FIR and MIR frequency ranges,

most either harden or remain constant in frequency as the temperature is decreased, although nearly half of the multiplets have one or two low-energy components that soften as part of the increased splitting of the mode at low T. We conclude that although some minor aspects of the behavior of the counterion are unique in the fulleride salt, most behaviors are consistent and thus are probably unrelated to the presence of the fullerene anion.

To summarize, we find that the T dependences of a few C_{60}^- modes of $(Ph_4As)_2ClC_{60}$ exhibit subtle behavioral changes near 200 K and some modes soften with decreasing temperature, usually associated with increased mode splitting. We discuss the anomalous softening of the 1386 cm^{-1} mode below, and here address the question of a possible T-induced transition near 200 K. The small magnitude of T-induced changes rules out a possible symmetry change in the cage with temperature, which would be manifest in marked changes in the splitting and complexity of the spectrum. In $(Ph_4P)_2IC_{60}$, several weak vibrational mode changes observed near 140 K were assumed to be associated with the sharp ESR g-factor anisotropy transition at the same temperature.[55] The same type of ESR transition occurs at 125 K in $(Ph_4As)_2ClC_{60}$,[40,57] whereas our strongest vibrational evidence is for a transition at 200 K. The disagreement in transition temperatures in $(Ph_4As)_2ClC_{60}$ suggests that the agreement between ESR and vibrational data in the isostructural material may be coincidental. The reported narrowing of the ^{13}C NMR line at $T=180$ K in $(Ph_4P)_2IC_{60}$, (Ref. 54) [not investigated in $(Ph_4As)_2ClC_{60}$] is in better agreement with our dominant transition temperature of 200 K. However, other reported transitions observed by ESR, NMR, and differential scanning calorimetry (DSC) all occur at lower T in $(Ph_4As)_2ClC_{60}$ than in $(Ph_4P)_2IC_{60}$,[57] making this agreement also suspect.

The weakness of the T-induced vibrational changes and lack of consistency with other results prevent us from shedding any light on the reported ESR transition in the $(Ph_4X)_2YC_{60}$ materials. The absence of an obvious transition in the vibrational data is not surprising, however. Although it was originally identified as a dynamic-to-static JT transition,[41] recent studies have attributed it to either an orientational glass transition (with static disorder below T_C),[36] an orientational ordering transition with ordered domains below T_C,[42] or to a cessation of pulsating deformations of a given distortion on a single cage.[33] Since none of the latter three requires a symmetry change of the cage, if any one of these is correct then the transition will be invisible in the vibrational spectrum unless there are simultaneous changes in the cage-lattice interactions. As discussed in Sec. III D, we expect these interactions in $(Ph_4As)_2ClC_{60}$ to be weak and have little effect on the intramolecular modes,[39] consistent with the weak temperature dependence we observe.

Although the observed temperature-dependent behavior in $(Ph_4As)_2ClC_{60}$ is generally weak, and thus no phase transition can be identified, the exceptional T-dependent softening of the intense 1386 cm^{-1} vibration deserves attention. Anticipating our assignments in the next section, we note that this mode is derived from the I_h C_{60} $T_{1u}(4)$ mode, which has the greatest double-bond stretching aspect of all the IR modes in I_h C_{60}.[80] Softening of vibrational frequencies with decreasing T is unexpected because the usual volume contraction with decreasing T causes bonds to stiffen and frequencies to harden.[81] This softening of the $T_{1u}(4)$-derived mode in $(Ph_4As)_2ClC_{60}$ is likely associated with an unusual expansion of the fullerene anion with decreasing T in this compound. According to the reported radii and bond lengths in an x-ray diffraction study of C_{60}^- in $(Ph_4As)_2ClC_{60}$ (Table I in Ref. 36), the average fullerene cage radius increases by 0.6% from 295 K to 120 K, driven in particular by a 1.4% increase in length of the double bonds between six-membered rings. (The distortion of the cage was below the resolution limit of the measurements.[36]) Lengthening the double bonds would be expected to soften the vibrations that involve stretching of these bonds, consistent with the T dependence we observe for the $T_{1u}(4)$-derived mode. Recently, Kwon *et al.* predicted a universal phenomenon of volume expansion in low-dimensional structures at low temperature due to vibrational and/or structural deformations that allow for the dominance of entropy over internal energy in the low-T regime.[82] More calculations are needed to determine if their model can quantitatively explain the observed cage expansion and mode softening of C_{60}^- in $(Ph_4As)_2ClC_{60}$.

C. Comparison of calculated and experimental spectra

In order to identify the particular distortion of C_{60}^- in $(Ph_4As)_2ClC_{60}$, we calculated the IR vibrations for the simulated distortions listed in Sec. II B, namely D_{5d}, D_{3d}, D_{2h}, $C_{2h,6}$, $C_{2h,5}$, and C_i. The calculated IR spectra of these six distortions are shown in Fig. 4, along with that of I_h C_{60} and the experimental C_{60}^- absorbance spectrum at $T=6$ K. For each of the D_{2h}, $C_{2h,5}$, and C_i symmetries, we calculated IR spectra for multiple sets of equilibrium atomic positions (see the discussion in Sec. II B); for each of these three symmetries, a selected spectrum is shown, but the alternate calculated spectra were quite similar in each case. The spectral region shown is from 300 to 700 cm^{-1}, which encompasses all experimental C_{60}^- modes identified in the FIR region and one MIR positively identified C_{60}^- doublet that has no overlapping counterion modes. The lower-symmetry calculated spectra appear to correspond better with the experimental spectrum; however, as discussed in Sec. II B, we primarily use the calculated frequencies, and only an order-of-magnitude intensity comparison from these spectra, when making assignments.

In Table I we present the experimental frequencies in the 300–700 cm^{-1} region, and compare them with the calculated frequencies for the two C_{60}^- symmetries that are ultimately preferred by our comparisons of theory and experiment, including the geometry comparison presented in Sec. III D. Table I also shows how the calculated vibrational mode patterns can be expanded in terms of the calculated modes of I_h C_{60}; we refer to the I_h C_{60} modes as the "parent" vibrational modes of the lower-symmetry C_{60}^- modes. In this spectral region there are four groups of calculated modes: those with $H_{1u}(1)$ parents, those with mixed $H_u(2)-T_{1u}(1)$ parentage, those with $T_{1u}(2)$ parents, and those with $H_u(3)$ parents. Most calculated C_{60}^- modes are derived from the single-

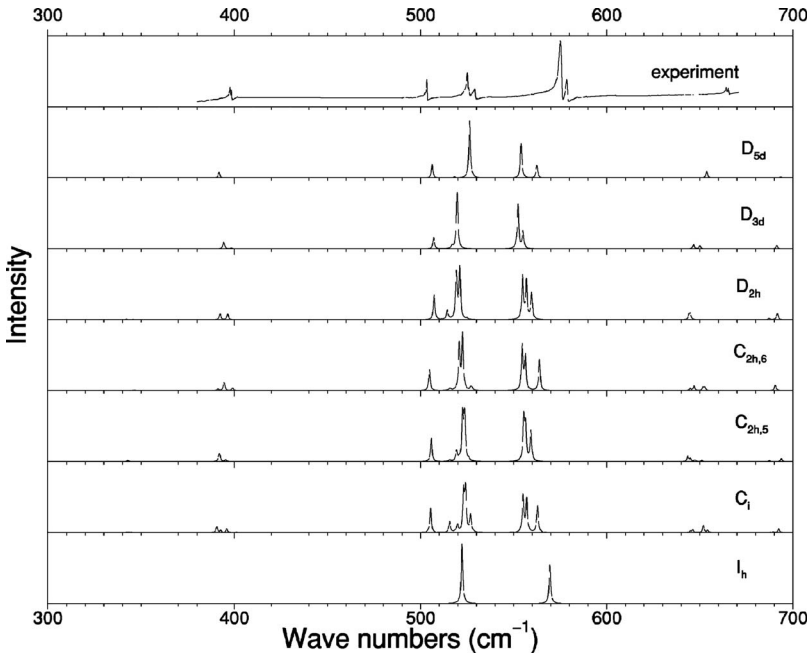

FIG. 4. Vertically offset calculated absorbance spectra of D_{5d}, D_{3d}, D_{2h}, $C_{2h,6}$, $C_{2h,5}$, and C_i C_{60}^-, as well as I_h C_{60}, compared with the experimental C_{60}^- absorbance as determined from the transmittance of $(Ph_4As)_2ClC_{60}$. In the experimental spectrum, the counterion modes are removed and replaced by straight lines and a linear baseline is subtracted to remove the paraffin matrix absorption.

parent icosahedral mode having the nearest frequency, and the calculated splitting of vibrations derived from degenerate I_h C_{60} parent modes is generally small: 1–8 cm^{-1} in $C_{2h,5}$ symmetry and 3–10 cm^{-1} in C_i. The significant exception is the region of calculated frequencies between 506 and 526 cm^{-1}, in which $T_{1u}(1)$ and $H_u(2)$ parent symmetries are strongly mixed, presumably due to the close proximity of the parent modes in the I_h C_{60} spectrum. In $C_{2h,5}$ C_{60}^-, five of the eight calculated modes contain more than a 10% contribution from the nondominant parent symmetry (four of the eight for C_i C_{60}^-). Furthermore, the calculated downshift of the lowest frequency $T_{1u}(1)$-derived component is an unexpectedly large 16 cm^{-1} (from 522 to 506 cm^{-1} in both symmetries). Large splittings and shifts have been found before for the severely-distorted covalently bonded balls in the high-pressure high-temperature C_{60} polymers,[59–61] but seem surprising for the small molecular JT distortion of the isolated singly charged anion.

In order to quantitatively determine which distortion best matches the experimental vibration spectrum, we first assigned individual calculated modes of a given distortion to the experimental C_{60}^- features. Since several of the distortion spectra have many more calculated modes than experimental features, we established a set procedure[83] for assigning the experimental peaks to the calculated modes. We then determined the average error (defined in the caption of Table I) of the calculated vibrational frequencies for each symmetry distortion.

Some distortions have too *few* calculated modes, so that physically reasonable assignments for all positively identified C_{60}^- features cannot be made; those distortions are eliminated immediately. D_{5d} symmetry is eliminated because its H_u-derived modes are all singlets, whereas we observe doublet features at typical H_u frequencies (Table I). The D_{3d} distortion is also eliminated if we take the 401.7 cm^{-1} small peak and 573.0 cm^{-1} shoulder to be components of C_{60}^- features, since triplet splitting of these features is not replicated in the D_{3d} $H_u(1)$- and $T_{1u}(2)$-derived modes. None of the distortions has a calculated mode that can reasonably be assigned to the ambiguous shoulder at 502.7 cm^{-1} so it remains unassigned and does not serve to distinguish among the different symmetries. When we do include the other two ambiguous C_{60}^- modes at 401.7 and 573 cm^{-1} in our assignments, we determine average errors of 2.0%, 1.8%, 1.6%, and 1.6% for the D_{2h}, $C_{2h,5}$, $C_{2h,6}$, and C_i distortions, respectively. If we do not assign the ambiguous C_{60}^- modes, the D_{3d} distortion is no longer automatically eliminated and has an error of 2.0%. In this case, the errors for the others are 2.0%, 1.7%, 1.4%, and 1.4%, respectively. The estimated uncertainties in all the average errors are $\leqslant$0.06%, as determined by error calculations on multiple equivalent distortions.[84] The $C_{2h,6}$ and C_i distortions are thus slightly preferred by the quantitative vibrational comparison, indicating that the C_{60}^- cage is of lower symmetry than any of the I_h direct subgroup (D_{5d}, D_{3d}, and D_{2h}) distortions. As discussed in Sec. III D, however, a geometric comparison eliminates the $C_{2h,6}$, D_{3d}, and D_{2h} distortions, while consideration of the lattice symmetry points to a $C_{2h,5}$ or C_i distortion. Thus, Table I compares the frequency assignments of the C_i and $C_{2h,5}$ distorted cages.

We successfully assign many of the experimental C_{60}^- modes based on the calculated spectra, with only minor differences between the $C_{2h,5}$ and C_i distortions. The surprising appearance (noted above) of a $T_{1u}(1)$-derived mode at 506 cm^{-1} in the calculated spectra is now appealing because it has a clear experimental counterpart at 503.5 cm^{-1} [Fig. 3(b)], a feature which was previously unidentified in the $(Ph_4P)_2IC_{60}$ spectrum.[55] The narrow doublet (possible triplet) at 398 cm^{-1} [Fig. 3(a)] is seen to be of $H_u(1)$ parentage, silent in neutral C_{60} but newly activated in a lower symmetry cage. If we take the shoulder at 573 cm^{-1} to be a C_{60}^- mode [Fig. 3(d)] rather than neglect it as a fine-structure feature (see discussion in Sec. III A), then the experimental feature is consistent with the calculated $T_{1u}(2)$-derived triplet be-

tween 555 and 563 cm^{-1}. The doublet at 665 cm^{-1} [Fig. 2(b)] is almost certainly $H_u(3)$ derived. More uncertainty exists for the exact assignments of the 525 and 529 cm^{-1} features, due to the many mixed $H_u(2)$-$T_{1u}(1)$-derived modes. As noted before, of the features identified in this work as C_{60}^- vibrations, only the ambiguous low-energy shoulder at 502.7 cm^{-1} has no possible assignment among our calculated modes. In contrast, many calculated features are missing from the experimental spectrum, probably because the actual intensities make them too weak to be observed. Some of the $T_{3u}(1)$- and $G_u(1)$-derived modes may be obscured by strong counterion modes.

As we found previously in work on neutral C_{60} vibrations,[75] our calculated frequencies in this region are consistently lower than the experimental ones. For neutral isolated I_h C_{60}, our frequencies in this region range from 0–3.5 % low, with an average of 1.2%, consistent with the errors shown in Table I. The one exception is the aforementioned strongly downshifted $T_{1u}(1)$-derived mode (at 505.8 cm^{-1} for $C_{2h,5}$ and 505.2 cm^{-1} for C_i), which has a calculated frequency slightly higher (less than 0.5%) than the peak to which it is assigned.

Although we do not attempt to assign in detail the multiplet splittings of the 1175 and 1387 cm^{-1} features because of their overlap with counterion modes, they have obvious parentage in the $T_{1u}(3)$ and $T_{1u}(4)$ I_h C_{60} fundamental modes. We calculate fivefold splitting of $T_{1u}(3)$ (mixed with nearby H_u and T_{3u} modes), consistent with the observed multiplet in Fig. 2(b) (minus the fine structure). The strong experimental $T_{1u}(4)$-derived feature at 1386 cm^{-1} is downshifted 41 cm^{-1} from its location in I_h C_{60}. Such charge-induced softening and intensity enhancement has been observed previously in $(Ph_4P)_2IC_{60}$[46] and in the A_nC_{60} compounds[85] and leaves little doubt as to its identification.

The FIR vibrational spectrum of the JT-distorted isolated C_{60}^- cage in $(Ph_4As)_2ClC_{60}$ contrasts sharply with the spectra of the bonded distorted balls of the high-pressure high-temperature (HPHT) C_{60} polymers and linear charged polymer, which also have been assigned using QMD calculations.[59–61] Vibrations of the *un*bonded mildly distorted balls in $(Ph_4As)_2ClC_{60}$ show much less splitting and mixing of parent modes, due to the much smaller degree of distortion, even though we find a lower cage symmetry than in the bonded C_{60} polymers. For example, no significant three-way mixing of I_h parent modes was calculated for $C_{2h,5}$ or C_i C_{60}^-, although such mixing of $T_{1u}(1)$, $T_{1u}(2)$, and $H_u(3)$ was common in the HPHT polymers.[60,61] Due to such multiple mixing, the modes of partial $T_{1u}(2)$ parentage are spread across more than 90 cm^{-1} in the orthorhombic C_{60} polymer (containing D_{2h} bonded balls[61]), whereas in the isolated C_{60}^- cage of $(Ph_4As)_2ClC_{60}$, $T_{1u}(2)$-derived modes are essentially of single parentage and are split only by 8 cm^{-1}. On the other hand, $T_{1u}(1)$-derived modes are mixed with $H_u(2)$ and appear over a range of 22 cm^{-1} in the C_i-distorted cage. This unexpectedly large splitting, despite the small distortion, may be related to the excess charge on the cage. When the charged and uncharged linear C_{60} chains were compared, it was found that the charged RbC_{60} chain exhibited wider separation of modes in this frequency region compared to the neutral HPHT C_{60} chain.[61] In sum, even for isolated cages in which the distortion magnitude is small, we find that the vibrational spectrum is complex and that first-principles QMD calculations yield a fuller understanding of the vibrational properties.

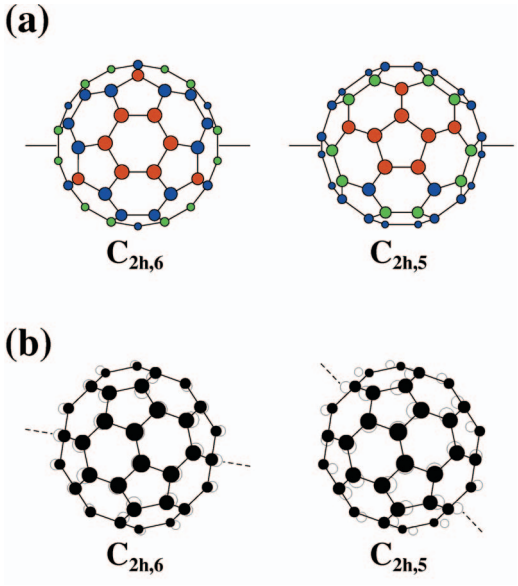

FIG. 5. (Color) Representations of the simulations of C_{60}^- distortions having $C_{2h,6}$ and $C_{2h,5}$ symmetries. (a) Qualitative color representations of the radial distortions. Red indicates atoms with an outward radial distortion, green indicates atoms with an inward radial distortion, and blue indicates atoms with comparatively small radial distortions (less than 0.005 Å). The extended lines indicate the positions of the C_2 symmetry axes. The $C_{2h,6}$ distortion is elongated along an axis through opposing sixfold rings, while the $C_{2h,5}$ distortion is elongated along an axis through opposing fivefold rings. (b) Quantitative representation of the distortions, magnified by factor of 20. Empty circles represent the distorted atomic positions; filled circles represent the calculated atomic positions of I_h-symmetric C_{60}^-. The extended lines (dashed) indicate the approximate positions of the axes of elongation. The views are along the C_2 symmetry axes. In (b), it is clear that the distortions are not purely radial, but have substantial tangential character. As explained in Sec. II B of the text, for neither $C_{2h,5}$ nor $C_{2h,6}$ can the atomic positions shown here, particularly away from the elongation axis, be regarded as unique.

D. Geometry of $C_{2h,5}$-distorted C_{60}^-

The approximate geometry of the distorted C_{60}^- cage in $(Ph_4As)_2ClC_{60}$ is known from the combined results of x-ray diffraction and ESR, which have identified the orientation and anisotropy of the cage within the lattice, respectively.[36,40] Visual inspection of Fig. 3 in Ref. 40 shows that the distorted cage is elongated along an axis penetrating two opposing five-membered rings.

Figure 5(a) qualitatively displays the radial aspect of our calculated $C_{2h,6}$ and $C_{2h,5}$ distortions and Fig. 5(b) shows the displacements of the atoms projected onto the plane of the page, on a scale enhanced by a factor of 20. In the $C_{2h,6}$ cage, the elongation axis penetrates two opposing six-membered

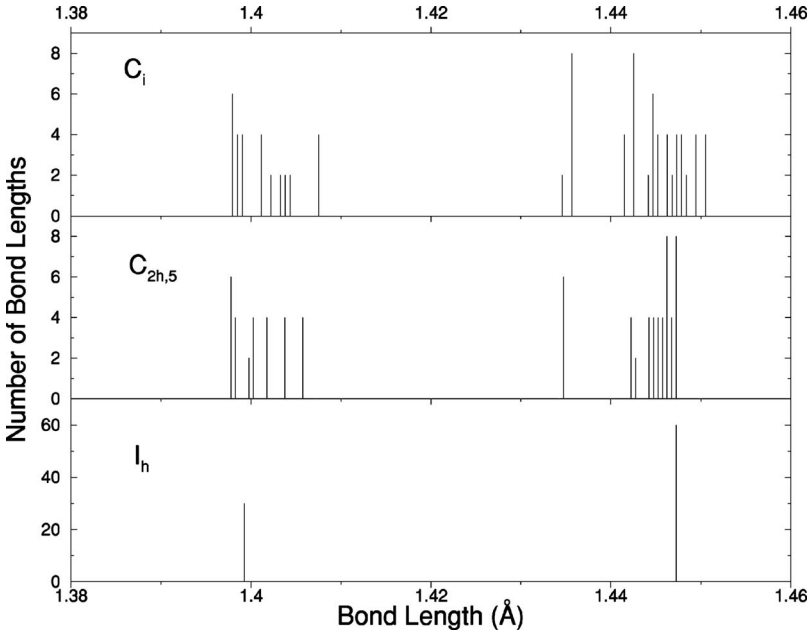

FIG. 6. Calculated bond-length distributions for neutral I_h C_{60} and for C_i and $C_{2h,5}$ C_{60}^-. The bond lengths of the distorted C_{60}^- cages are clustered around the two I_h C_{60} bond lengths.

rings, whereas the $C_{2h,5}$ cage is elongated along an axis that penetrates two opposing five-membered rings. The C_i cage (not shown) is also elongated along an axis through five-membered rings. Of special note is the fact that the elongation axis does not coincide with the C_2 symmetry axis in either of the C_{2h} symmetry cages, as can be seen in Fig. 5(b). In that figure, each C_2 axis is directed out of the page, passing through the center of the double bond between six-membered rings, while the elongation axis is in the plane of the page. Both the $C_{2h,6}$ and $C_{2h,5}$ distortions contrast sharply with our higher symmetry distorted structures, D_{5d}, D_{3d}, and D_{2h}, for which the elongation axis always coincides with the principal symmetry axis, as found in previous calculations.[31] The distinction between the elongation axis and the symmetry axis in the C_{2h} cages can be understood by observing that each of the $C_{2h,6}$- and $C_{2h,5}$-distorted cage shapes is a perturbation on a higher-symmetry distorted cage, $C_{2h,6}$ being derived from D_{3d} and $C_{2h,5}$ from D_{5d}. In each case, the elongation axis is preserved whereas all symmetry elements are destroyed except for a mirror plane containing the elongation axis and a perpendicular twofold rotation axis.

In Fig. 5(b), the C_{2h} cages are displayed with an orientation chosen deliberately to coincide with the cage orientation in Fig. 3 of Ref. 40, so that the $C_{2h,5}$ cage may be overlaid on the latter, showing the significant agreement between the calculated and experimentally determined distortions. The C_i cage shows equally good agreement. In contrast, the $C_{2h,6}$, D_{3d}, and D_{2h} cages have an incorrect elongation axis and can be immediately dismissed. Kodama *et al.*[33] also found that the C_{60}^- cage in $(Ph_4P)_2YC_{60}$ materials has C_{2h} or C_i symmetry, based on ESR experiments and *ab initio* molecular orbital calculations. The authors of Ref. 40 concluded that the distortion was of D_{2h} symmetry, based on ESR data that were gathered by rotation of the sample around two perpendicular axes and revealed a nonaxial g tensor. An even lower symmetry distortion could not be excluded, however, due to the limited angular range of the ESR measurements,[40] and the lower-symmetry (C_{2h} or C_i) cage is a central result of the present paper.

Changes in individual bond lengths can be discerned qualitatively from the atomic displacements as shown in Fig. 5(b). The distorted C_{60}^- cage produces a variety of bond lengths clustered around the two I_h bond lengths: the short double bonds between six-membered rings and the longer single bonds on the edges of five-membered rings. For C_i and $C_{2h,5}$ C_{60}^-, the bond lengths are presented quantitatively in Fig. 6, which shows the range of calculated bond lengths of the distorted cages as well as the two bond lengths of I_h C_{60}. The greatest bond length change between either of the distorted C_{60}^- cages and the I_h C_{60} ball is the shortening of a few single bonds by 0.012–0.013 Å in the $C_{2h,5}$ cage. All other changes are less than or equal to 0.01 Å, and all changes are less than 1%. It is noteworthy that such tiny percent changes in the bonding configuration of this highly symmetric molecule have such a profound effect on the vibrational properties, attesting to the value of vibrational spectroscopy for investigating symmetry changes of C_{60}.

Our calculations do not distinguish energetically among the different possible JT distortions of C_{60}^-, consistent with the picture that the isolated molecule could dynamically sample all of the possible distortions, even at low temperature.[2,31,32] ESR and x-ray diffraction results, however, indicate static distortion and orientational disorder of C_{60}^- in $(Ph_4As)_2ClC_{60}$,[36,40] implying that interactions between the fullerene anion and surrounding counterions stabilize a given distortion and orientation of the cage at low T. It is therefore important to consider the lattice site symmetry at the location of the cage. In a static perfect lattice, any point symmetry operation of the cage must also be a point symmetry operation for the lattice. In our case, with static orientational disorder present, this can be achieved by averaging over the disorder. In $(Ph_4As)_2ClC_{60}$, the C_{60}^- cages are located at $4/m$ (C_{4h}) sites,[34] in which the fourfold rotation axis lies along the unit cell c axis and the mirror plane is parallel to the ab plane. The most exact match of C_{60}^- molecular symmetry to the lattice site symmetry is provided by a C_{2h} distortion of the ball, with the C_2 axis aligned along the cell

c axis and the cage mirror plane coincident with the mirror plane of the lattice. These conditions are met by our simulated $C_{2h,5}$ distortion, oriented as shown in Fig. 5(b), with the lattice *c* axis pointing out of the page as in Fig. 3 of Ref. 40. A 50-50 random mixture of the two static energetically equivalent 90° orientations of the cage (consistent with ESR data[40]) provides the additional twofold rotation to restore, on average, the fourfold lattice site symmetry. The C_i distorted cage lacks the mirror plane and rotational symmetry of the lattice site, but a fourfold orientational disorder of the cage with equal random occupancy of 0, 90, 180, and 270 degree rotations around the crystal *c* axis also will effectively restore those symmetries, on average. Such additional orientational disorder at 180° would not have been observable by recent x-ray diffraction experiments, since it would require a detectable distortion which was not achieved.[36] Thus, our simulated C_i distorted cage, with its rotation and elongation axes similarly oriented as for $C_{2h,5}$, and with the fourfold orientational disorder just described, can also satisfy the symmetry constraints of the lattice. In contrast, D_{5d}, D_{3d}, and D_{2h} distorted cages all have too high symmetry for that required by the site.

We now review the case for each of the $C_{2h,5}$ and C_i distortions. The C_i vibrational comparisons are slightly more favorable than those for $C_{2h,5}$ (Table I), although the comparisons are limited by the lack of accurate calculated intensities. Both $C_{2h,5}$ and C_i have an elongation axis through five-membered rings that is consistent with the ESR data.[40] Since lattice symmetry considerations do not distinguish definitively between the two symmetry cages, neither can be ruled out on that basis. The C_i cage requires somewhat more elaborate orientational disorder than the $C_{2h,5}$ cage, however, which makes it seem less probable. A C_i distorted cage might also be argued against on the grounds that standard JT theory does not lead to a C_i distortion of C_{60}^-.[2] As discussed in Sec. II B, however, the actual molecular configuration in the sample is determined by the growth kinetics, and is not limited to JT-theory approximations. Summarizing, the symmetry arguments seem to favor $C_{2h,5}$, while our experimental-theoretical vibrational comparisons slightly favor C_i, and neither can be ruled out at present.

It is interesting to compare our system to other materials with statically distorted C_{60}^- cages. In the case of the ordered fulleride salts $[PPN^+]_2C_{60}^{2-}$ and $[Ni(C_5Me_5)_2^+][C_{60}^-]CS_2$, which have known C_{60}^- distortions, the cage symmetries do in fact match the lattice site symmetry, as required by lattice periodicity. These are materials with significant cage-lattice interactions, as indicated by the suppression of orientational disorder.[24,25] Our system, $(Ph_4As)_2ClC_{60}$, has presumably weaker interactions, as indicated by the persistence of orientational disorder and smaller distortion of the C_{60}^- cage.[36] As we have seen, the orientational disorder allows for a lower symmetry cage than the lattice site symmetry. In the case of the ferromagnet TDAE-C_{60}, the cages reside at sites of inversion (C_i) symmetry and the system is ordered at low temperature.[20] Thus our present results suggest that the C_{60}^- anion would have a C_i-distorted equilibrium configuration in this material. In fact, since our simulated C_i distortion has an elongation axis through opposing five-membered rings, it agrees with the proposed antiferro-rotative structure of Fig. 5(a) in Ref. 20 in which the elongated cage aligns alternately along the [001] and [110] directions. Since the C_{60}^- cage is oriented within the TDAE-C_{60} lattice such that five-membered rings also face nearly the same [001] and [110] directions,[20] a C_i distortion is consistent with the proposed elongation orientations.

IV. CONCLUSION

We have made a combined experimental-theoretical investigation of the vibrational properties of $(Ph_4As)_2ClC_{60}$, which contains the isolated C_{60}^- anion in a nearly isotropic environment.[34] The experimental high-resolution C_{60}^- vibrational spectrum is complex, indicative of a reduced cage symmetry, and requires the complementary information of our QMD calculations to assign the C_{60}^- modes. Calculated mode splittings are surprisingly wide in the region of mixed $T_{1u}(1)$- and $H_u(2)$-derived vibrations and are confirmed in the experimental spectrum. Anomalous softening (4 cm^{-1}) of the $T_{1u}(4)$-derived mode occurs with decreasing temperature, but other *T*-dependent changes in the vibrational properties are too weak to identify a temperature-induced ordering transition. Comparing the experimental and calculated vibrational spectra allows us to identify a C_{2h} or C_i symmetry of the distorted singly charged cage, with C_i slightly favored. The static orientational disorder of C_{60}^- cages in $(Ph_4As)_2ClC_{60}$[36,40] requires us to consider if the distortion matches the lattice site symmetry. Although both C_{2h} and C_i cages can satisfy the C_{4h} site symmetry by averaging over random orientational disorder, the required disorder is somewhat more elaborate for the C_i cage. On this basis, C_{2h} is slightly favored, and we therefore rule out neither symmetry molecule. Both of our preferred simulated C_{60}^- cage structures are elongated along an axis penetrating opposing five-membered rings, in agreement with the experimental elongation determined by *g*-factor anisotropy of C_{60}^- in $(Ph_4As)_2ClC_{60}$.[40] Calculated maximum bond length changes in the C_{2h} and C_i cages are not more than 0.013 Å; it is therefore not surprising that structural investigations have been unable to detect the distortion directly.[36]

Note added in proof. In the final version of this paper, we inadvertently omitted a mention of vibrational studies that found specific reduced symmetries of the charged cages in the A_4C60 compounds.[9,86]

ACKNOWLEDGMENTS

We thank Jürgen Gmeiner for assistance in growing samples and K. Kamarás for a careful reading of and helpful comments on this paper. V.C.L. acknowledges support from the Henry Luce Foundation and the National Science Foundation.

*Email address: vclong@colby.edu
†Email address: gary.adams@asu.edu
‡Email address: john.page@asu.edu

[1] I. B. Bersuker, *The Jahn Teller Effect and Vibronic Interactions in Modern Chemistry* (Plenum Press, New York, 1984).
[2] C. C. Chancey and M. C. M. O'Brien, *The Jahn Teller Effect in* C_{60} *and Other Icosahedral Complexes* (Princeton University Press, Princeton, NJ, 1997).
[3] J. L. Dunn, Phys. Rev. B **69**, 064303 (2004).
[4] L. Forró and L. Mihály, Rep. Prog. Phys. **64**, 649 (2001).
[5] O. Gunnarsson, Rev. Mod. Phys. **69**, 575 (1997).
[6] O. Gunnarsson, J. E. Han, E. Koch, and V. H. Crespi, Struct. Bonding (Berlin) **114**, 71 (2005).
[7] C. M. Varma, J. Zaanen, and K. Raghavachari, Science **254**, 989 (1991).
[8] M. Lannoo, G. A. Baraff, M. Schlüter, and D. Tomanek, Phys. Rev. B **44**, 12106 (1991).
[9] G. Klupp, K. Kamarás, N. M. Nemes, C. M. Brown, and J. Leao, Phys. Rev. B **73**, 085415 (2006).
[10] P.-M. Allemand, K. C. Khemani, A. Koch, F. Wudl, K. Holczer, S. Donovan, G. Grüner, and J. D. Thomson, Science **253**, 301 (1991).
[11] D. Arčon and K. Prassides, Struct. Bonding (Berlin) **100**, 129 (2001).
[12] D. Mihailovič, D. Arčon, P. Venturini, R. Blinc, A. Omerzu, and P. Cevc, Science **268**, 400 (1995).
[13] T. Kawamoto, Solid State Commun. **101**, 231 (1997).
[14] B. Narymbetov, A. Omerzu, V. V. Kabanov, M. Tokumoto, H. Kobayashi, and D. Mihailovič, Nature (London) **407**, 883 (2000).
[15] T. Kambe, Y. Nogami, and K. Oshima, Phys. Rev. B **61**, R862 (2000).
[16] K. Mizoguchi, M. Machino, H. Sakamoto, T. Kawamoto, M. Tokumoto, A. Omerzu, and D. Mihailovič, Phys. Rev. B **63**, 140417(R) (2001).
[17] P. Jeglič, R. Blinc, T. Apih, A. Omerzu, and D. Arčon, Phys. Rev. B **68**, 184422 (2003).
[18] V. Brouet, H. Alloul, S. Garaj, and L. Forro, Struct. Bonding (Berlin) **109**, 165 (2004).
[19] R. Blinc, P. Jeglič, T. Apih, J. Seliger, D. Arčon, and A. Omerzu, Phys. Rev. Lett. **88**, 086402 (2002).
[20] M. Fujiwara, T. Kambe, and K. Oshima, Phys. Rev. B **71**, 174424 (2005).
[21] P. Dahlke and M. J. Rosseinsky, Chem. Mater. **14**, 1285 (2002).
[22] C. A. Kuntscher, G. M. Bendele, and P. W. Stephens, Phys. Rev. B **55**, R3366 (1997).
[23] I. D. Hands, J. L. Dunn, and C. A. Bates, Phys. Rev. B **73**, 235425 (2006).
[24] P. Paul, Z. Wei, R. Bau, P. D. W. Boyd, and C. R. Reed, J. Am. Chem. Soc. **116**, 4145 (1994).
[25] W. C. Wan, X. Liu, G. M. Sweeney, and W. E. Broderick, J. Am. Chem. Soc. **117**, 9580 (1995).
[26] N. Manini, E. Tosatti, and A. Auerbach, Phys. Rev. B **49**, 13008 (1994).
[27] S. Sookhun, J. L. Dunn, and C. A. Bates, Phys. Rev. B **68**, 235403 (2003).
[28] M. C. M. O'Brien, Phys. Rev. B **53**, 3775 (1996).
[29] J. Ihm, Phys. Rev. B **49**, 10726 (1994).
[30] J. L. Dunn and C. A. Bates, Phys. Rev. B **52**, 5996 (1995).
[31] N. Koga and K. Morokuma, Chem. Phys. Lett. **196**, 191 (1992).
[32] G. B. Adams, O. F. Sankey, J. B. Page, and M. O'Keeffe, Chem. Phys. **176**, 61 (1993).
[33] T. Kodama, M. Kato, K. Mogi, M. Aoyagi, and T. Kato, Mol. Phys. Rep. **18/19**, 121 (1997).
[34] A. Pénicaud, A. Peréz-Benítez, R. Gleason V., E. Muñoz P., and R. Escudero, J. Am. Chem. Soc. **115**, 10392 (1993).
[35] V. V. Gritsenko, O. A. Dyachenko, G. V. Shilov, N. G. Spitsyna, and E. B. Yagubskii, Russ. Chem. Bull. **46**, 1878 (1997).
[36] K. Pilz, A. Jobst, E. Lam, J. Lüdecke, J. Bao, W. Bietsch, and M. Schwoerer, Z. Kristallogr. **217**, 78 (2002).
[37] U. Bilow and M. Jansen, J. Chem. Soc., Chem. Commun. **4**, 403 (1994).
[38] M. Scudder and I. Dance, J. Chem. Soc. Dalton Trans. **1998**, 3155.
[39] M. S. Dresselhaus, G. Dresselhaus, and P. C. Eklund, *Science of Fullerenes and Carbon Nanotubes* (Academic Press, New York, 1996).
[40] W. Bietsch, J. Bao, J. Ludecke, and S. van Smaalen, Chem. Phys. Lett. **324**, 37 (2000).
[41] B. Gotschy, M. Keil, H. Klos, and I. Rystau, Solid State Commun. **92**, 935 (1994).
[42] P. Launois, R. Moret, N.-R. de Souza, J. A. Azamar-Barrios, and A. Pénicaud, Eur. Phys. J. B **15**, 445 (2000).
[43] U. Becker, G. Denninger, V. Dyakonov, B. Gotschy, and H. Klos, Europhys. Lett. **21**, 267 (1993).
[44] V. Dyakonov, G. Rösler, B. Gotschy, and A. Hirsch, Synth. Met. **56**, 3214 (1993).
[45] H. Klos, W. Brütting, A. Schilder, W. Schütz, B. Gotschy, G. Völkel, B. Pilawa, and A. Hirsch, in *Progress in Fullerene Research*, edited by H. Kuzmany, J. Fink, M. Mehring, and S. Roth (World Scientific, Singapore, NJ, 1994), pp. 297–300.
[46] K. Kamarás, K. Matsumoto, M. Wojnowaki, E. Schönherr, H. Klos, and B. Gotschy, in *Progress in Fullerene Research* (Ref. 45), pp. 357–361.
[47] G. Völkel, A. Pöppl, J. Simon, J. Hoentsch, S. Orlinskii, H. Klos, and B. Gotschy, Phys. Rev. B **52**, 10188 (1995).
[48] K. Kamarás, D. B. Tanner, L. Forró, M. C. Martin, L. Mihály, H. Klos, and B. Gotschy, J. Supercond. **8**, 621 (1995).
[49] B. Gotschy and G. Völkel, Appl. Magn. Reson. **11**, 229 (1996).
[50] W. Scheinast, A. Schilder, W. Schütz, and B. Gotschy, in *Fullerenes and Fullerene Nanostructures*, edited by H. Kuzmany, J. Fink, M. Mehring, and S. Roth (World Scientific, Singapore, NJ, 1996), pp. 544–547.
[51] V. N. Semkin, N. G. Spitsina, S. Król, and A. Graja, Chem. Phys. Lett. **256**, 616 (1996).
[52] A. Graja, V. N. Semkin, N. G. Spitsina, and S. Król, in *Electrical and Related Properties of Organic Solids*, edited by R. W. Munn, A. Miniewicz, and B. Kuchta (Klewer Academic, Dordrecht, the Netherlands, 1997), Vol. 24, pp. 259–278.
[53] J. L. Sauvajol, A. Graja, L. Firlej, and S. Król, J. Mol. Struct. **436-437**, 19 (1997).
[54] W. Schütz, A. Schilder, W. Bietsch, B. Gotschy, and M. Schwoerer, in *Molecular Nanostructures*, edited by H. Kuzmany, J. Fink, M. Mehring, and S. Roth (World Scientific, Singapore, NJ, 1998), pp. 275–278.
[55] V. C. Long, J. L. Musfeldt, K. Kamarás, A. Schilder, and W. Schütz, Phys. Rev. B **58**, 14338 (1998).
[56] M. Polomska, J.-L. Sauvajol, A. Graja, and A. Girard, Solid State Commun. **111**, 107 (1999).
[57] W. Bietsch, J. Bao, P. Medick, and S. Traßl, in *Electronic Prop-*

erties of Novel Materials—Molecular Nanostructures (American Institute of Physics, Melville, NY, 2000), Vol. 544, pp. 46–49.
[58] K. Kamarás, J. M. Walner, D. B. Tanner, V. C. Long, J. L. Musfeldt, A. Schilder, and W. Schütz, http://solidstate.physics.sunysb.edu/lees2002/speakers/proceedings.html.
[59] V. C. Long, J. L. Musfeldt, K. Kamarás, G. B. Adams, J. B. Page, Y. Iwasa, and W. E. Mayo, Phys. Rev. B **61**, 13191 (2000).
[60] Z.-T. Zhu, J. L. Musfeldt, K. Kamarás, G. B. Adams, J. B. Page, V. A. Davydov, L. S. Kashevarova, and A. V. Rakhmanina, Phys. Rev. B **65**, 085413 (2002).
[61] Z.-T. Zhu, J. L. Musfeldt, K. Kamarás, G. B. Adams, J. B. Page, L. S. Kashevarova, A. V. Rakhmanina, and V. A. Davydov, Phys. Rev. B **67**, 045409 (2003).
[62] K. M. Mackay, D. B. Sowberry, and W. C. Young, Spectrochim. Acta, Part A **24**, 611 (1968).
[63] G. Socrates, *Infrared Characteristic Group Frequencies: Tables and Charts*, 2nd ed. (Wiley, New York, 1994).
[64] O. F. Sankey and D. J. Niklewski, Phys. Rev. B **40**, 3979 (1989).
[65] G. B. Adams, J. B. Page, O. F. Sankey, K. Sinha, J. Menéndez, and D. R. Huffman, Phys. Rev. B **44**, 4052 (1991).
[66] G. B. Adams, O. F. Sankey, J. B. Page, and M. O'Keeffe, Science **256**, 1792 (1992).
[67] G. B. Adams, J. B. Page, O. F. Sankey, and M. O'Keeffe, Phys. Rev. B **50**, 17471 (1994).
[68] G. B. Adams, J. B. Page, and M. O'Keeffe, Chem. Phys. Lett. **228**, 485 (1994).
[69] S. Lebedkin, H. Rietschel, G. B. Adams, J. B. Page, F. H. Hennrich, H.-J. Eisler, M. M. Kappas, and W. Krätschmer, J. Chem. Phys. **110**, 11768 (1999).
[70] G. B. Adams and J. B. Page, in *Fullerene Polymers and Fullerene-Polymer Composites*, edited by P. C. Eklund and A. M. Rao (Springer Verlag, Berlin, 2000), p. 185.
[71] M. Canonico, G. B. Adams, C. Poweleit, J. Menéndez, J. B. Page, G. Harris, H. P. van der Meulen, J. M. Calleja, and J. Rubio, Phys. Rev. B **65**, 201402(R) (2002).
[72] G. B. Adams, M. O'Keeffe, O. F. Sankey, and J. B. Page, in *Novel Forms of Carbon*, edited by C. L. Renschler, J. J. Pouch, and D. M. Cox (Materials Research Society, Pittsburgh, 1993), Vol. 270, p. 103.
[73] M. O'Keeffe, G. B. Adams, and O. F. Sankey, Phys. Rev. Lett. **68**, 2325 (1992).
[74] G. B. Adams, M. O'Keeffe, A. A. Demkov, O. F. Sankey, and Y. M. Huang, Phys. Rev. B **49**, 8048 (1994).
[75] J. Menéndez and J. Page, in *Light Scattering in Solids*, edited by M. Cardona and G. Guntherodt (Springer, Heidelberg, 2000), p. 27.
[76] D. H. Whiffen, J. Chem. Soc. **1956**, 1350.
[77] W. R. McWhinnie, J. Chem. Soc. A **1966**, 889.
[78] J. B. Orenberg, M. D. Morris, and T. V. Long, II, Inorg. Chem. **10**, 933 (1971).
[79] V. C. Long, J. L. Musfeldt, K. Kamarás, A. Schilder, and W. Schütz (unpublished).
[80] R. E. Stanton, J. Phys. Chem. **92**, 2141 (1988).
[81] P. M. A. Sherwood, *Vibrational Spectroscopy of Solids* (Cambridge University Press, Cambridge, 1972).
[82] Y.-K. Kwon, S. Berber, and D. Tománek, Phys. Rev. Lett. **92**, 015901 (2004).
[83] Modes are naturally grouped by parentage (see Table I); we consider this parentage grouping when assigning modes to experimental features. Within a given parentage grouping, the weakest modes are eliminated from consideration if (1) the calculated intensity of the weak mode is an order of magnitude less than the calculated intensity of any mode still in consideration and (2) the number of modes in consideration is greater than or equal to the number of experimental features which have to be assigned within that parentage grouping. In addition, no assigned mode can be an order of magnitude weaker than a mode which remains unassigned. Within the above limitations, modes within each parentage grouping are assigned so as to minimize the average error in frequency between theory and experiment.
[84] The small magnitude of the estimated uncertainties is indicative of the insignificance of the differences between multiple equivalent distortions. The choice of which versions of the $C_{2h,5}$ and C_i distortions to present in Figs. 4–6, and Table I is essentially arbitrary; the selected versions show the greatest possible contrast between the $C_{2h,5}$ and C_i assignments.
[85] T. Pichler, R. Winkler, and H. Kuzmany, Phys. Rev. B **49**, 15879 (1994).
[86] K. Kamarás, G. Klupp, D. B. Tanner, A. F. Hebard, N. M. Nemes, and J. E. Fisher, Phys. Rev. B **65**, 052103 (2000).